5.3×10^{-7} cm^2 s^{-1} within an experimental error of 10% from the linear plot of the relaxation time τ_s of the decay profile of the diffraction intensity vs. d^2, the square of the grating spacing. The value is larger than D_{slow} by a factor of about 5, even if we account for the difference in viscosity between THF and benzene. This kind of discrepancy has been found in the D_{slow} data of Amis and Han as mentioned already. At present we believe that the slow mode does not reflect the reptation motion of a single chain but does reflect coordinated motion of many polymer chains which gives rise to a long-lived concentration fluctuation.

Acknowledgment. N.N. is grateful to Prof. H. Yu of the University of Wisconsin for giving him an opportunity to make FRS measurements on a THF solution of a binary blend.

References and Notes

(1) de Gennes, P.-G. "Scaling Concepts in Polymer Physics"; Cornell University Press: Ithaca, NY, 1979.
(2) Nystrom, B.; Roots, J. *J. Macromol. Sci., Rev. Macromol. Chem.* **1980**, *C19*, 35.
(3) Callaghan, P. T.; Pinder, D. N. *Macromolecules* **1980**, *13*, 1085.
(4) Klein, J. *Macromolecules* **1978**, *11*, 852.
(5) Amis, E. J.; Han, C. C. *Polym. Commun.* **1982**, *23*, 1403.
(6) Brown, W.; Johnsen, R. M.; Stilbs, P. *Polym. Bull.* **1983**, *9*, 305.
(7) Nishio, I.; Wada, A. *Polym. J.* **1980**, *12*, 145.
(8) Mathiez, P.; Mouttet, C.; Weisbuch, G. *J. Phys. (Paris)* **1980**, *41*, 519.
(9) Yu, T. L.; Reihanian, H.; Jamieson, A. M. *Macromolecules* **1980**, *13*, 1590.
(10) Amis, E. J.; Janmey, P. A.; Ferry, J. D.; Yu, H. *Macromolecules* **1983**, *16*, 441.
(11) Leger, L.; Hervet, H.; Rondelez, F. *Macromolecules* **1981**, *14*, 1732.
(12) Chang, T.; Yu, H. *Macromolecules* **1984**, *17*, 115.
(13) Miyaki, Y.; Einaga, Y.; Fujita, H. *Macromolecules* **1978**, *11*, 1180.
(14) Nemoto, N.; Makita, Y.; Tsunashima, Y.; Kurata, M. *Macromolecules* **1984**, *17*, 425.
(15) Nemoto, N.; Tsunashima, Y.; Kurata, M. *Polym. J.* **1981**, *13*, 827.
(16) Tsunashima, Y.; Nemoto, N.; Kurata, M. *Macromolecules* **1983**, *16*, 1184.
(17) Adam, M.; Delsanti, M. *Macromolecules* **1977**, *10*, 1229.
(18) Wesson, J. A.; Noh, I.; Kitano, T.; Yu, H. *Macromolecules* **1984**, *17*, 782.
(19) Osaki, K.; Nishizawa, K.; Kurata, M. *Macromolecules* **1982**, *15*, 1068.
(20) Fukuda, M.; Fukumoto, M.; Kato, Y.; Hashimoto, T. *J. Polym. Sci., Polym. Phys. Ed.* **1974**, *12*, 871.
(21) Daoud, M.; Cotton, J. P.; Farnoux, B.; Jannink, G.; Sarma, G.; Benoit, H.; Duplessix, R.; Picot, C.; de Gennes, P.-G. *Macromolecules* **1975**, *8*, 804.
(22) Oyama, T.; Shiokawa, K.; Baba, K. *Polym. J.* **1982**, *14*, 667.
(23) de Gennes, P.-G. *Macromolecules* **1976**, *9*, 594.
(24) Chu, B.; Nose, T. *Macromolecules* **1980**, *13*, 122.
(25) Brown, W. *Macromolecules* **1984**, *17*, 66.

A Laser Light Scattering Study on Molecular Weight Distribution of Linear Polyethylene

John W. Pope and Benjamin Chu*

Department of Chemistry, State University of New York at Stony Brook, Stony Brook, Long Island, New York 11794-3400. *Received January 19, 1984*

ABSTRACT: Time-average and time-dependent intensity of light scattered by linear polyethylene (LPE), Dutch State Mines sample L30-4-6, in a good organic solvent, 1,2,4-trichlorobenzene at 135 °C, was measured as a function of polymer concentration at scattering angles between 35 and 145°. Molecular properties determined were the z-average radius of gyration, $\langle R_g^2\rangle_z^{0.5} = 50$ nm, the z-average hydrodynamic radius, $\langle R_h^{-1}\rangle_z^{-1} = 27$ nm, the weight-average molecular weight, $\langle M\rangle_w = 570$, the weight distribution, $F_w(M)$, and the second virial coefficient, $A_2 = 1.5 \times 10^{-3}$ g^{-2} mL mol. The main purpose of this article was to determine $F_w(M)$ for a LPE based on $\langle M\rangle_w$, $\langle R_g^2\rangle_z$, A_2, and the characteristic line width distribution $G(\Gamma)$ computed from an inverse Laplace transform of the measured single-clipped time correlation function, $G_k^{(2)}(\tau)$. We have demonstrated this nonintrusive technique to be particularly useful in obtaining an approximate $F_w(M)$ for polydisperse synthetic high polymers which are difficult to characterize by more established analytical techniques such as gel permeation chromatography (GPC).

I. Introduction

1.1. Overview. Several studies[1,2] have attempted to determine the molecular weight distribution (MWD) of commercial linear polyethylene (LPE). It is also possible to extract the MWD of a polydisperse sample from combined measurements of static and dynamic light scattering.[3,4] The MWD is asscessible from light scattering due to the influence of the molecular weight distribution on dynamic measurements. For polydisperse samples, time correlation function (or power spectrum) profile analysis permits us to relate the distribution of translational diffusion coefficients with the molecular weight distribution provided we have taken into account interparticle interactions and molecular self-interference, i.e., virial coefficients and $P(K,R_g)$, respectively.

We approximate the power spectrum (or time correlation function) as a linear sum of basis functions with distinct characteristic decay times. Each characteristic decay time is related to a particular diffusion coefficient and, thus, to a particular molecular weight fraction. In addition to dynamic light scattering, we call upon static light scattering to determine the weight-average molecular weight, the z-average radius of gyration, and the second virial coefficient of the polymer–solvent system. The combination of both static and dynamic measurements allows a complete determination of the MWD.

This article will describe the combined dynamic and static light scattering experimental method used to characterize LPE. A yet more interesting problem is to investigate how LPE differs from long-chain branched polyethylene (BPE) of the same molecular weight. The present study is used to provide the experimental benchmark of LPE in order to begin the study of BPE, which is in progress.

The light scattering technique is similar to more established GPC by virtue of its use of the hydrodynamic radius

0024-9297/84/2217-2633$01.50/0

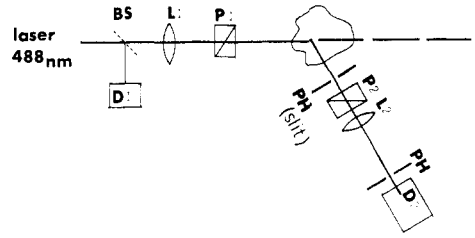

Figure 1. Schematic diagram of optial geometry: BS, beam splitter; D1, solar cell; D2, photomultiplier (approximately 1 m from sample); L1, 0.55-m lens at focal distance from sample; L2, 0.15-m lens at focal distance from rear PH; P1 and P2, Glan–Thompson polarizers; PH (slit), pinhole for dynamic measurement (0.020–0.013-in. diameter) (slit for static measurement (0.020 in.) PH, pinhole to define angular uncertainty (0.012-in. diameter).

(or volume) to distinguish molecular species present in solution but is in contrast since the polymer is never physically fractionated.

1.2. Polymer System. The samples studied were dilute solutions of linear polyethylene (LPE) in 1,2,4-trichlorobenzene (TCB) at 135 °C. At small scattering angles, the LPE molecules may be treated as Brownian particles[5] undergoing translational diffusion through a continuous medium. The LPE molecules are polydisperse and, as a result, have a distribution of translational diffusion rates. The molecular weight distribution (MWD) of LPE is sufficiently broad to permit a transform from the measured intensity autocorrelation function $G_k^{(2)}(\Gamma)$ to the distribution of diffusion coefficients $G(D)$ by means of a multiexponential analysis of the first-order electric field correlation function $g^{(1)}(t)$. We have succeeded in determining an approximate distribution of diffusion coefficients, $G(D)$, and in transforming $G(D)$ into a distribution of molecular weights, $F(M)$. Furthermore, we were able to confirm the validity of our procedure by comparing the derived MWD with the literature MWD measured by GPC. The determination of a MWD for this LPE sample demonstrates how our method for characterization of polymers dissolved in a hazardous solvent at elevated temperatures complements the more standard techniques such as GPC.

1.3. Optical Geometry. Figure 1 shows a schematic diagram of the top view of our light scattering spectrometer. From left to right we have an argon ion laser operating at $\lambda_0 = 488.0$ nm with roughly vertically polarized light in the TEM_∞ Gaussian spatial mode. A beam splitter BS diverts light to a solar cell D1, which monitors the relative intensity arriving at the LPE sample. The lens L1 and polarizer P1 define the beam position, size, and polarization within the sample. The detection optics select the scattering volume, angle, angular divergence, and polarization of scattered light reaching the photomultiplier tube D2.

For dynamic measurements only the photomultiplier detector at D2 is used. Our correlator computes the single-clipped autocorrelation function, $G_k^{(2)}(t)$, which is closely related to the complex-valued normalized electric field autocorrelation function $g^{(1)}(t)$. If we treat the photocounts as a Gaussian random variable[6-10]

$$G_k^{(2)}(t) = A(1 + b|g^{(1)}(t)|^2) \tag{1-1}$$

The constant b includes the fact that D2 is not an ideal point detector and b is therefore a function of the detection optics.

II. Theoretical Background

2.1. Static Light Scattering (Following the Huglin Text[11]). The excess intensity of light scattered at a given angle from a dilute polymer solution can be written as

$$\frac{Hc}{R_{vv}(\theta)} = \frac{1}{\langle M\rangle_w}\left(1 + \frac{K^2\langle R_g^2\rangle_z}{3}\right) + 2A_2c \tag{2-1}$$

where

$$H = \left(\frac{4\pi^2n^2}{N_A\lambda^4}\right)\left(\frac{\partial n}{\partial c}\right)^2$$

with n, $R_{vv}(\theta)$, λ ($\equiv\lambda_0/n$), c, A_2, $\langle R_g^2\rangle$, and M being, respectively, the solvent index of refraction, the Rayleigh ratio, the wavelength of light in the scattering medium, the concentration, the second virial coefficient, the z-average square of the radius of gyration, and the weight-average molecular weight. $\partial n/\partial c = 0.109$ [mL g^{-1}] for our LPE in TCB. We have also assumed that our measured value of A_2, 1.5×10^{-3} [mL mol g^{-2}], is independent of M.

For a Gaussian random coil, the particle scattering factor has the form[12]

$$P(X) = \frac{2}{X^2}(\exp(-X) + X - 1) \tag{2-2}$$

where $X = (KR_g)^2$ with $K = (4\pi/\lambda)\sin(\theta/2)$. Equation 2-2 is used to approximate the particle scattering factor for non-Gaussian LPE molecules. It happens that the higher molecular weights in our LPE molecular weight distributions yield an X value of about 1 at 40°; thus the more accurate eq 2-2 is utilized for the dynamic light scattering molecular weight transform described in section 2.3.

By means of eq 2-1, the graphical method due to Zimm[13] yields the physical properties $\langle M\rangle_w$, $\langle R_g^2\rangle_z^{0.5}$, and A_2. To derive an apparent radius of gyration at finite concentration, $\langle R_g\rangle^*_z$, we let

$$\langle R_g^2\rangle^*_z = \frac{\langle R_g^2\rangle_z}{1 + 2A_2cM_w} \tag{2-3}$$

One numerical constant necessary for the calculation of $\langle M\rangle_w$ and A_2 needs to be discussed, namely, the incremental change of the index of refraction vs. concentration $(\partial n/\partial c)_{T,P}$. The value of $\partial n/\partial c$ for LPE in TCB at 135 °C has been measured[1] and is essentially constant over the entire MWD studied. This implies that the intensity scattered by a single LPE molecule scales as $M^2P(X)$.

In calibrating our instrument for absolute intensity measurements, we used the static structure factor for benzene, $R_{uu}(90)$.[14-18] Second, we approximately know that, by taking into account the detector solid angle acceptance as a function of index of refraction for the detection geometry used in Figure 1,[19] we can express the relationship between the relative scattered intensity I^* and the absolute quantity R_{vv} as

$$R_{vv}(\theta) = CI^*(\theta) \tag{2-4}$$

where

$$C = R_{vv\ \mathrm{benzene}}n_{\mathrm{solvent}}/(I^*_{\mathrm{benzene}}n_{\mathrm{benzene}})$$

Equation 2-4 uses constants all at the same temperature, scattering angle, and wavelength.

The value of $R_{vv}(90)$ for benzene at 135 °C was only recently reported[20] by us. Conversion between R_{vv} and R_{uu} occurs via simple Cabannes ratios of temperature-dependent depolarization constants.[21] The primary reference $R_{vv}(90)$ of benzene at 25 °C and 488 nm is

$$R_{vv}(90) = 3.14 \times 10^{-5}\ [\mathrm{cm}^{-1}]$$

2.2. Dynamic Light Scattering. In this section we tacitly consider only dilute solution conditions and thus

ignore such complications as multiple scattering and gel formation. We also assume that the scattering geometry is arranged so number fluctuations and heterodyning do not contribute to the dynamic properties. In the low-X limit, just as in static light scattering, the intramolecular polymer segment motions contribute little to the overall changes occurring in K space.[22] In this low-X limit we need only consider the molecular LPE center-of-mass motions. The functional form for the molecular pair distribution of Brownian particles is available[23] and results in a direct relationship between the translational diffusion coefficient, D [cm^2 s^{-1}], and the intensity spectrum, $S(\omega)$. The property $g^{(1)}(t)$ is thus related directly to the measured net single-clipped autocorrelation function $(G_k^{(2)}(t) - A)$.[6-10]

Given the fact that translational diffusion for one molecular size will produce a single-exponential decay with characteristic frequency Γ for $g^{(1)}(t)$, adding additional independent molecules of differing sizes into the scattering volume will result in a weighted sum of exponentials as follows:

$$g^{(1)}(t) \propto \sum w_i \exp(-\Gamma_i t) \qquad \text{for molecules } i \tag{2-5}$$

where the absolute value signs are implied on $g^{(1)}(t)$ and the weighting factor w_i is proportional to the time-average intensity scattered by species i at angle θ. At infinite dilution, only M and $P(X)$ are included in this weighting term

$$w_i = M_i^2 P(X_i) \tag{2-6}$$

No n_i term appears in eq 2-6 since the summation is over molecules and not over molecular weight fractions. Combination of eq 2-5 and 2-6 forms the basis of the molecular weight transform. One calculates a normalized distribution of line widths, $G(\Gamma)$, through the inverse Laplace transform of the measured $g^{(1)}(t)$.

$$g^{(1)}(t) = \int_0^\infty G(\Gamma) \exp(-\Gamma t)\, d\Gamma \tag{2-7}$$

The characteristic decay time Γ scales according to the relation[23]

$$\Gamma = DK^2 \tag{2-8}$$

If one includes polydispersity effects and assumes $P(X)$ to be unity, we have $\langle\Gamma\rangle = \langle D\rangle_z K^2$, where the angle brackets around Γ indicate the mean Γ value defined by the moments of $G(\Gamma)$; i.e., $\langle\Gamma\rangle = \int_0^\infty \Gamma G(\Gamma)\, d\Gamma$. In more general terms of the molecular weight distribution

$$\langle\Gamma\rangle = K^2 \frac{\int_0^\infty D(M)P(X)F(M)M^2\, dM}{\int_0^\infty P(X)F(M)M^2\, dM} \tag{2-9}$$

Then $\langle\Gamma\rangle$ is no longer equal to $\langle D\rangle_z K^2$ when $P(X) \neq 1$.

2.3. A Molecular Weight Transform. The final transform to be dealt with leads us from the distribution of diffusion coefficients, $G(D)$, to the underlying number-average molecular weight distribution, $F_n(M)$. Two relationships are central to this transformation. First, molecular weight, M, must be stated as a function of diffusion coefficient D. Second, some approximate form for the molecular self-interference term, $P(X)$, must be stated in terms of D. It should be remembered that once we have an estimate for $G(\Gamma)$ we will also know the distribution $G(D)$ if eq 2-8 is valid, i.e., if we are measuring only translational molecular diffusion in $g^{(1)}(t)$.

At this point we should be more precise and mathematically define our terms. Let

$$G(\Gamma) = \sum_j^J a_j \delta(\Gamma - \Gamma_j) \tag{2-10}$$

$$G(D) = \sum_j^J b^+{}_j \delta(D - D_j) \tag{2-11}$$

and

$$F_n(M) \propto \sum_j^J n_j \delta(M - M_j) \tag{2-12}$$

where the following conditions hold: $\sum^J a_j = 1, \Gamma_j/\Gamma_{j+1}$ is a constant for the model distributions, $b^+{}_j \propto a_j$, $\sum n_j$ does not necessarily equal 1, and n_j is proportional to the number of molecules in the jth fraction of the MWD.

The density function has an associated cumulative distribution function, $\mathbf{F}_n(M)$, defined by

$$\mathbf{F}_n(M) = \int_0^M F_n(M)\, dM \Big/ \int F_n(M)\, dM \tag{2-13}$$

In discrete distributions, $\langle M\rangle_n = \sum M_j n_j / \sum n_j$, $\langle M\rangle_w = \sum M_j^2 n_j / \sum M_j n_j$, $\langle M\rangle_z = \sum M_j^3 n_j / \sum M_j^2 n_j$, and $\langle R_g^2\rangle_z = \sum (R_g^2)_j M_j^2 n_j / \sum M_j^2 n_j$, where special attention should be paid to the use of the index j, which denotes the collection of representative monodisperse fractions approximating $F_n(M)$. It is asserted that the continuum of molecules i may be approximated by a limited number, J, of monodisperse species.

Each representative species j will have an associated molecular weight M_j and form factor $P(X_j)$. The jth contribution to $g^{(1)}(t)$ is directly proportional to the number of molecules in the jth fraction, n_j, multiplied by the weighting factor w_j. Thus

$$|g^{(1)}(t)| = \frac{\sum^J [n_j M_j^2 P(X_j)] \exp(-\Gamma_j t)}{\sum^J [n_j M_j^2 P(X_j)]} \tag{2-14}$$

It is possible to see how this model for $g^{(1)}(t)$ relates to our model for $G(\Gamma)$ by substituting eq 2-10 into the Laplace integral relationship, eq 2-7, yielding

$$|g^{(1)}(t)| = \sum_j^J a_j \exp(-\Gamma_j t) \tag{2-15}$$

where each of the a_j contributions is linearly independent with

$$a_j = n_j M_j^2 P(X_j) / \sum^J [n_j M_j^2 P(X_j)] \tag{2-16}$$

From eq 2-16 we immediately notice that $n_j \propto a_j / M_j^2 P(X_j)$. We shall collect all the proportionality constants by writing

$$n_j = a_j^* / [M_j^2 P(X_j)] \tag{2-17}$$

where the unnormalized line width distribution $G^*(\Gamma)$ has the form

$$G^*(\Gamma) = \sum_j^J a_j^* \delta(\Gamma - \Gamma_j) \tag{2-18}$$

$F_n(M)$, defined by eq 2-12, is obtained from eq 2-17 once we know the set of values $\{a_j^*, M_j, P(X_j) | j = 1, J\}$. The unnormalized line width distribution, i.e., $\{a_j^*\}$, is related to the experimentally measured net single-clipped correlation function by the Laplace transform, eq 2-7, such that

$$(Ab)^{1/2} |g^{(1)}(t)| = \sum_j^J a_j^* \exp(-\Gamma_j t) \tag{2-19}$$

where $\sum^J a_j^* = (Ab)^{1/2}$.

In our experiments, values for $G_k^{(2)}(t)$ were available only at equally spaced intervals of delay time t. The statistical counting noise at each data point of $G_k^{(2)}(t)$ is approximately proportional to $1/A^{1/2}$ and is thus roughly equal for all measured $G_k^{(2)}(t)$ values.[24] Consequently the pa-

rameters a_j^* can be calculated from $(G_k^{(2)}(t) - A)^{1/2} = (Ab)^{1/2}|g^{(1)}(t)|$ by an equally weighted linear least-squares (L^2) or absolute linear (L^1) norm fitting algorithm. For this experiment we chose a full derivative Marquardt L^2 fitting routine from the International Math and Statistics Library (routine ZXSSQ modified to use an analytic form for the Jacobian matrix). The Marquardt routine was used to minimize problems encountered during the inversion of the constant matrix of this linear problem where the Γ_j's are fixed parameters during the fitting procedure. There are, of course, several more direct routes[25,26] to the solution of this generalized matrix inversion problem.

It suffices to say that simulated data, similar to the LPE correlation function, yield the predicted a_j^* values upon completion of the Marquardt fitting method. Therefore, we make the crucial assertion that the calculated a_j^* values are unbiased estimators of the true $G(\Gamma)$. We begin the molecular weight transform by taking $D_j = \Gamma_j/K^2$ and by setting $b_j^* = a_j^*$. We now have $G^*(D)$, provided that only translational diffusion determines $g^{(1)}(t)$. At infinite dilution, there are several empirical relations available:

$$D_j = k_D M_j^{\alpha_D} \tag{2-20}$$

$$(R_g^2)_j = k_R M_j^{\alpha_R} \tag{2-21}$$

and for completeness we have the intrinsic viscosity as

$$[\eta] = k_\eta M^{\alpha_\eta} \tag{2-22}$$

We first extrapolate our measured diffusion coefficients to zero concentration where we have taken k_d to be independent of M in dilute solution

$$\langle D\rangle_z = \langle D_0\rangle_z(1 + k_d c) \tag{2-23}$$

From this point on we shall assume that the D_j values used in relation to eq 2-20 are the D_j values extrapolated to infinite dilution by means of eq 2-23. A plot of $\langle D\rangle_z$ vs. c yields the proportionality constant $(1 + k_d c)$. It should be noted that branched polyethylene and other polymers having a molecular shape which depends on M require a functional form for k_d with respect to M. In practice, we cannot decrease the concentration indefinitely to avoid this extrapolation, since the signal-to-noise ratio of $G_k^{(2)}(t)$ may become too unfavorable to allow a sufficiently detailed inverse Laplace transform.

In our system of LPE at 135 °C in TCB we have α_η equal to aproximately 0.72 from the studies cited in ref 27. We assume that the scaling exponents may be taken as independent of M over the range of our MWD. In this case we have[28]

$$\alpha_D = -(1 + \alpha_\eta)/3 \tag{2-24}$$

$$\alpha_R = (1 + \alpha_\eta)/3 \tag{2-25}$$

and all we require to determine $\{M_j|j = 1, J\}$ is the preexpoential factor k_D. If we assume that $P(X)$ is unity, we may immediately calculate k_D since we know $\langle M\rangle_w$ from our static light scattering measurements.

$P(X)$ is not unity, however, and we are therefore forced to calculate the correct k_D in an iterative fashion. By taking the first approximation for k_D, we can now calculate $\{M_j|j = 1, J\}$ and $\{P(X_j)|j = 1, J\}$, where $P(X_j)$ is given by eq 2-2 and X_j is available by assuming an approximate k_R in eq 2-21. Thus we have made an initial estimate of $\{M_j|j = 1, J\}$ and $\{P(X_j)|j = 1, J\}$, which means we know an initial approximation for $F_n(M)$. From this trial $F_n(M)$ we may calculate the resulting $\langle M\rangle_w$ and $\langle M\rangle_z$ values in order to achieve better values for k_D and k_R in eq 2-20 and 2-21. Through successive iterations we arrive at a $\langle M\rangle_w$ calculated from $F_n(M)$ which is consistent with the measured $\langle M\rangle_w$ from static light scattering. In addition, we arrive at calculated values for k_D and k_R.

One unemphasized point is the set of constraints necessary to carry out this transformation. First, we need $\langle M\rangle_w$ and $\langle R_g^2\rangle_z$ from static measurements. $\langle M\rangle_w$ ties down the value of k_D. A change in k_D will shift the calculated molecular weight distribution. We have chosen to plot $F_z(M)$, i.e., $F_n(M)M^2/\int F_n(M)M^2\, dM$, since this moment of the MWD is most closely related to $G(D)$. The relative magnitude of each representative fraction remains constant, independent of k_D, until we include the effect of $P(X_j)$, which is a function of k_R. The $\langle R_g^2\rangle_z$ constraint is seen to define the X_j values in terms of the M_j axis. We recalculate the k_R value at each iteration by using the calculated $\langle M\rangle_z$, the measured $\langle R_g^2\rangle_z$, and the assumed α_R in eq 2-21.

In review, the distribution of diffusion coefficients, $G(D)$, is directly related to the MWD, $F_n(M)$. Static light scattering predicts that each representative D_j in $G(D)$ will be emphasized by a factor $M_j^2P(X_j)$ relative to the desired $F_n(M)$. To determine M_j and X_j as a function of D_j we require some knowledge of the relations between M vs. D and M vs. R_g. Given the static properties $\langle M\rangle_w$ and $\langle R_g^2\rangle_z$ and the value of α_D we are able to determine the preexponential constants k_D and k_R, which in turn define our desired $F_n(M)$. If eq 2-20 and 2-21 are known from previous measurements, $F_n(M)$ can be directly computed from $G(D)$. Furthermore, at small scattering angles $P(X)$ approaches unity and we only need eq 2-20, the Mark–Houwink equation, to define the transform from $G(D)$ to $F_n(M)$.

III. Experimental Sample Preparation

HPLC-grade 1,2,4-trichlorobenzene (TCB) was vacuum distilled and checked for purity on a standard analytical gas chromatograph. BHT (2,6-di-*tert*-butyl-4-methylphenol) was then added to the TCB to make a 0.05 wt % antioxidant solution. This solution was subsequently degassed and handled under a nitrogen atmosphere during the LPE sample dissolution. The LPE samples prepared with this solvent under a nitrogen atmosphere showed no signs of oxidation, i.e., yellowing or $\langle R_g^2\rangle_z$ change, for periods of at least 24 h at 135 °C.

Special care needs to be exercised when working with TCB at 135 °C. TCB has a flash point of 126 °C. TCB is also a health hazard when inhaled or absorbed through the skin, being linked to liver damage. Finally, TCB will dissolve most common plasticware, i.e., polyethylene, at 135 °C.

Due to our solvent nature and the necessarily high experimental temperature, only metal, Teflon, and glass were used as components in our stock solution filtration apparatus. Two types of filters were used to exclude dust from our light scattering solutions: solid Teflon (0.5 μm, Millipore) for cold solvent filtration, and fritted glass (4–5 μm, Corning fine grade, instead of the popular sintered metal filters) for hot stock solution filtration.

The sample preparation was carried out under a nitrogen atmosphere. Degassed TCB (with BHT) was first filtered into clean dust-free light scattering cells. Ulfiltered solvent was used to prepare a stock solution of LPE in TCB. The resulting stock concentration was nominally 4 mg of LPE/mL of TCB at 135 °C for the two sets of six samples prepared of the DSM L30-4-6 linear polyethylene standard sample. The stock solution was allowed to mildly stir for at least 4 h at 140 °C to ensure sample homogeneity. The stock solution was then filtered into light scattering cells containing known amounts of filtered and degassed TCB containing antioxidant BHT. In this manner we have a dilution scheme which permits us to prepare a set of solutions ranging in concentration from the stock concentration to about one-tenth this initial value.

Some pertinent details about the filtration procedure are as follows. All hot LPE in TCB transfers were made through Teflon tubings (Cole-Palmer, Chicago, IL) which fit tightly over 19-gauge surgical needles mounted to Luer joint hubs (Popper and Sons, New Hyde Park, NY). The temperature near the Teflon tubes

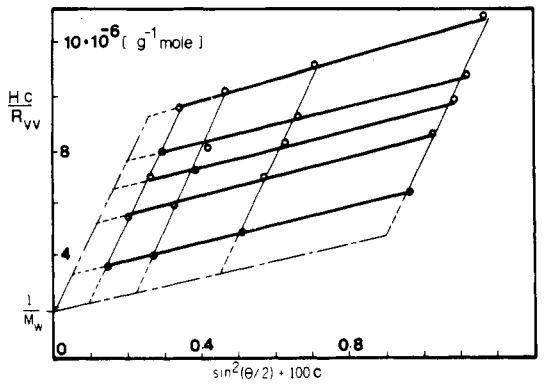

Figure 2. Zimm plot for DSM L30-4-6 LPE in TCB.

was carefully monitored to avoid stress-induced LPE crystalization. A 10-mL glass syringe was fitted with a valve (Pharmacia part no. SR-1, Piscataway, NJ) which allowed us to store the stock solution drawn out of a 25-mL Erlenmeyer stock flask while attaching the glass filter equipped with suitable joints. With this apparatus we were able to directly filter our stock solution into light scattering cells. Each cell was made of precision 1.0-cm-o.d. round-bottom Pyrex tubing (Wilmad Glass, Buena, NJ) which was fitted at the top with a glass joint (Kontes no. 570250-9005) and matching Teflon cap with Viton seal (Kontes no. 570250-9004).

By using this apparatus we were able to prepare and seal our LPE solutions with acceptably small dust and oxygen contamination. Once the stock solution had been diluted we used a biological test tube vortexing mixer to ensure mixing, taking care not to allow our solution to contact the cap region of the cell. After completion of each experiment, all glassware was cleaned with refluxing tetrachloroethylene, a good polyethylene solvent. No attempts were made to reuse the Teflon tubing.

IV. Experimental Results

4.1. Static Light Scattering Results. Our LPE in TCB polymer–solvent solutions produced a several-kilohertz photon counting frequency while using 0.14-W incident laser power at 488 nm. The observed ratio of LPE sample intensity to background solvent intensity was greater than 2 for most of our LPE solution concentrations, which ranged from 0.5 to 3.0 mg/mL. Our intensity data were measured to a counting precision of 1%.

At each scattering angle we accumulated the average intensity, $I_{vv}^*(\theta)$, over a 12-s measurement interval. We confirmed that the normalized intensity measured during each 1.2-s subinterval of the total measurement did not fluctuate by more than 10% of $I_{vv}^*(\theta)$. In such a fashion we have excluded the possibility of large dust particles contaminating our data.

The instrument was calibrated for absolute intensity with the following calibration samples: benzene (Bz), tolulene, 1,2,4-trichlorobenzene (TCB), ethanol/Bz, and methanol/Bz. Alignment with a benzene reference sample was found to be constant about $\theta = 90°$, ±1% for the quantity $I_{vv}^*(\theta) \sin(\theta)$, in the range $\theta = 35$–$145°$ and $T = 25$–135 °C. $R_{vv}(90)$ for Bz at 135 °C and 488 nm was 6.91×10^{-5} [cm^{-1}] from the work done in ref 20, which is consistent with our experimentally determined ratio in eq 2-5 and the known value of $R_{vv}(90)$ for Bz at 25 °C.

A Zimm plot for the DSM L30-4-6 LPE sample dissolved in TCB is shown in Figure 2. The average static properties for this linear polyethylene standard as measured over two sets of solutions, each set containing six concentrations, are $\langle R_g^2 \rangle_z^{0.5} = 50$ nm, $A_2 = 1.5 \times 10^{-3}$ ($(0.5$–$2.0) \times 10^{-3}$ Welzen) [mL mol g^{-2}], and $\langle M \rangle_w = 570 \times 10^3$ (530×10^3 DSM data).

We used $\delta n/\delta c = 0.109$ mL/g,[1] $n = 1.529$, $\rho = 1.315$ g/mL, and $\eta = 5.5 \times 10^{-3}$ P[29] for TCB at 135 °C and $\lambda_0 = 488$ nm. We noted that the viscosity values tabulated in ref 30 are in millipoise, rather than in centipoise as they have reported. The index of refraction for TCB at 135 °C was obtained by taking the ratio $(n - 1)/\rho$ to be temperature independent. Table I gives the preliminary line width results for three different sample concentrations. The mean of the distribution is seen to change, as predicted by eq 2-23, but the normalized variance of the distributions remains at approximately 0.2.

Table I
Concentration Dependence of $G(\Gamma)$[a]

	concn, mg/mL		
	1.75	1.15	0.58
Double Exponential			
mean, $\langle\Gamma\rangle$, kHz	5.10	4.70	4.15
normalized variance, $\langle\Gamma^2\rangle/\langle\Gamma\rangle^2 - 1$	0.28	0.20	0.22
Second-Order Cumulants			
$\langle\Gamma\rangle$, kHz	4.75	4.54	4.01
normalized variance	0.18	0.15	0.17
Third-Order Cumulants			
$\langle\Gamma\rangle$, kHz	5.08	4.69	4.18
normalized variance	0.28	0.21	0.25

[a] Scattering angle = 40°.

4.2. Distribution of Line Widths. To calculate a distribution of molecular translational diffusion coefficients, $G(D)$, we transform the measured function $G_k^{(2)}(t)$ into a representative distribution of line widths $G(\Gamma;\mathbf{a})$. Several conditions severely limit the resolution obtainable in any estimate of the true $G(\Gamma)$. For instance, the nature of the statistics for $G_k^{(2)}(t)$, i.e., the noise on our data, is imprecisely known. If we did know $g^{(1)}(t)$ exactly, $g^{(1)}(t)$ would still be bandwidth limited and the fundamental problem of a numerical integral transform with an exponential kernal would remain.

The current literature dealing with this data inversion problem of Freholm equations of the first kind (e.g., Bertero, McWhirter, Tikhonov, and Miller)[26,31-34] begins to quantify which methods of approximating $G(\Gamma)$ are optimal and what confidence levels on calculated $G(\Gamma;\mathbf{a})$ are consistent with experimental $G_k^{(2)}(t)$ data.

There are several considerations which allow us to restrict the class of possible solutions for $G(\Gamma)$. Physically, $G(\Gamma)$ and Γ must both be positive. Experimentally, $G_k^{(2)}(t)$ is bandwidth limited, which bounds the range of Γ. And, from sampling theory considerations, we know $G(\Gamma)$ is representable by a discrete distribution which samples $G(\Gamma)$ with finite resolution in Γ-space. A maximal description for $G(\Gamma)$ is a weighted sum of Dirac δ functions as defined by

$$G(\Gamma;\mathbf{a}) = \sum^{J} a_j \delta(\Gamma - \Gamma_j) \qquad (2\text{-}10)$$

where

$$\sum a_j = 1 \quad \text{(normalization constraint)} \qquad \text{(I)}$$

$$\Gamma_j/\Gamma_{j-1} = W \quad \text{(constant log } \Gamma \text{ spacing)} \qquad \text{(II)}$$

We have been more specific now and denoted the model function for $G(\Gamma)$ as $G(\Gamma;\mathbf{a})$, where $\mathbf{a}$ represents the independent parameters. Constraint II limits the resolution available in our calculated data.[31]

The calculated $G(\Gamma;\mathbf{a})$ is biased by our selection of sampling locations in Γ-space. As the number of independent parameters J is increased, the biasing is reduced. However, the uncertainty of our solution $\mathbf{a}$ must increase.

One approach to avoid this biasing, but to still retain a small number of independent variables, is to combine

several estimates for $G(\Gamma)$, with different samplings of Γ-space, into one composite distribution.[35] The composite "curve" consists of amplitudes **a** plotted vs. log Γ. Each of the independent estimates for $G(\Gamma)$ contributes J amplitudes to the composite $G(\Gamma;\mathbf{a})$, where this composite distribution now has N^*J amplitudes. N is the number of independent estimates for $G(\Gamma)$ by which we form the smoothed distribution. Each of these independent estimates use the same number of samplings, J, and the same sampling resolution in Γ-space, W. The only difference between samplings is the starting Γ_1 value used in eq 2-10.

For the independent estimates of $G(\Gamma)$ from our LPE data we determined that the maximum number of independent variables, J, is about 3. We also found that the maximum resolution, W, is about equal to 7/2. The choice of maximum independent parameters and minimal spacing was determined by fitting $G(\Gamma;\mathbf{a})$ using several combinations of these J and W parameters until we arrived at a selection which produced a physically expected smooth unimodal distribution. The chosen spacing directly effects the smoothness obtained for $G(\Gamma;\mathbf{a})$. Small spacings can result in large negative contributions in $G(\Gamma;\mathbf{a})$; i.e., the "independent" parameters a_j will actually become coupled in our fitting procedure if the spacing is too small. We have confirmed, by cumulants and double-exponential analysis of $G_k^{(2)}(t)$, that our $G(\Gamma)$ is sufficiently broad so that a $W = 7/2$ spacing will span only a fraction of the full range of $G(\Gamma)$. With the spacing chosen, the number of parameters, J, is then determined by the range of $G(\Gamma)$. If J is too large the sampled range in Γ-space will be too large, resulting in negative or insignificant contributions to $G(\Gamma;\mathbf{a})$ at the extreme values of $\{\Gamma_j | j = 1, J\}$.

The "smoothest" possible distribution $G(\Gamma;\mathbf{a})$ results when a minimum in the Euclidian norm of the solution vector **a** is found for a fixed number of independent parameters. This smoothing is equivalent to regularizing the inverse Laplace transform[32] and represents a limiting class of possible distributions which we may seek by this method. If an inidividual fit is not smooth, we have either too many independent parameters or an incorrect sampling interval.

We have recently found that the method of singular valued analysis (International Math and Statistics Library routine LSVDF) is most illuminating in determining the number of independent parameters obtainable from our data.[4] In fact, this method incorporates the probability that the number of independent basis functions is far too large for the precision of the experimental data, allowing us to use a model where we start with 20 samplings of Γ-space and immediately obtain an unbiased estimate for $G(\Gamma)$ in terms of linear combinations of the 20 Γ_j samplings. By this analysis we have confirmed[4] that $J = 3$ and $W = 7/2$ are conservative estimates of maximum independent parameters and resolution given our LPE data; i.e., the 5th-order singular valued decomposition solution appears to be the most detailed solution possible allowed by the noise on our data.

We analyzed the data here by combining three independent fits with $J = 3$ and $W = 7/2$ to yield a composite distribution as shown in Figure 3. We have plotted unnormalized coefficients, a_j^*, vs. log Γ. Each representative fit contributes three amplitudes to the figure. Since the sampling was done for each independent fit with a constant log Γ spacing of 5/4, corresponding to $W = 7/2$, we see that the 1st, 4th, and 7th points in Figure 3 resulted from one of the three fits. Similarly, we have the other two fits represented by the (2nd, 5th, 8th) and the (3rd, 6th, 9th) respective data points. The small Γ values correspond to

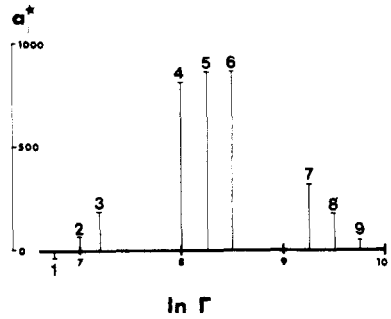

Figure 3. $G^*(\Gamma;\mathbf{a})$ for DSM L30-4-6 linear polyethylene. Concentration, 1.15 mg/mL; temperature, 135 °C; angle, 40°.

slow characteristic molecular diffusion and thus to large molecules in solution. At the large Γ values we have the other extreme of our molecular weight distribution represented; i.e., we have correspondingly small molecules. Knowing that the diffusion coefficient roughly scales as the square root of the molecular weight in eq 2-20 tells us that range of log M covered by Figure 3 is roughly twice the range in log Γ displayed. The general data fitting procedure used to obtain the final $G(\Gamma;\mathbf{a})$ in Figure 3 is as follows. We first estimated the mean and variance of $G(\Gamma)$ by a double-exponential four-parameter nonlinear least-squares criteria fit to $g^{(1)}(t)$. We modeled $g^{(1)}(t)$ by the following parameterized function:

$$g^{(1)}(t;\mathbf{p}) = p_1 \exp(-p_2 t) + p_3 \exp(-p_4 t) \qquad (4\text{-}1)$$

which corresponds to the following in Γ space:

$$G(\Gamma;\mathbf{p}) = p_1\delta(\Gamma - p_2) + p_3\delta(\Gamma - p_4) \qquad (4\text{-}2)$$

We also estimated the mean and variance of $G(\Gamma)$ by a cumulants analysis,[36] which calculates the moments of $G(\Gamma)$ by an analysis of the derivatives of $G_k^{(2)}(t)$ as t aproaches 0. The cumulants method relies upon a power series expansion about $\langle\Gamma\rangle$ and thereby is more accurate when describing symmetric narrow $G(\Gamma)$ distributions.

With $\langle\Gamma\rangle$ and $\langle\Gamma^2\rangle/\langle\Gamma\rangle^2 - 1$, i.e., the mean and normalized variance of $G(\Gamma)$, we may select a simple two-parameter continuous distribution to estimate the range $G(\Gamma)$ spans. Most notable of these simple distributions are the normal (Gaussian), Γ (χ^2 and others), and Poisson distributions. Once we have an approximate continuous or discrete (eq 4-2) distribution for $G(\Gamma)$, we have a starting range for Γ-space in eq 2-10.

For scaling to translational diffusion we have $K = 1.351 \times 10^5$ [cm^{-1}]. For hydrodynamic radius calculation we used the solvent viscosity $\eta = 5.5$ mP. From $G_k^{(2)}$ data at other angles, differing K values, we found $\langle\Gamma\rangle/K^2$ to be relatively constant, confirming we are truly measuring translational diffusion.

One trend of the line width distribution analysis was the higher variance obtained ($\mu_2/\bar{\Gamma}^2 = 0.42$) in a multiexponential analysis for $G(\Gamma;\mathbf{a})$ when compared to variances determined with a double-exponential ($\mu_2/\bar{\Gamma}^2 = 0.20$) or cumulants method ($\mu_2/\bar{\Gamma}^2 = 0.15$, second order). This is partially indicative of the long high molecular weight tail in $G(\Gamma;\mathbf{a})$, as shown by Figure 3, which represents an asymmetry in the MWD. The preliminary data analysis methods are not well suited to describe asymmetric distributions. The long tail would be more obvious if we plotted Figure 3 using Γ rather than log Γ.

We calculated $G(\Gamma;\mathbf{a})$ as described earlier using the preliminary $\langle\Gamma\rangle$ and $\langle\Gamma^2\rangle$ as a guide to an initial estimate for $G(\Gamma;\mathbf{a})$. After several iterations we chose $J = 3$ and $W = 7/2$ for our final data analysis, which resulted in Figure

3. To give this plot more physical sense, we write

$$G^*(D) = \sum b_j^* \delta(D - D_j) \quad (4\text{-}3)$$

where

$$\ln D_{0j} = \ln \Gamma_j - 2 \ln K - \ln (1 + k_d c) \quad (4\text{-}4)$$

$$a_j^* = b_j^* \quad (4\text{-}5)$$

Thus $G^*(D)$ is a shifted copy of Figure 3, the shift in log space for this sample being $22.1 = -2 \ln K - \ln (1 + k_d c)$. The normalization constraint I from eq 2-10 is never required for our analysis, and for clarity we have taken the liberty of interchanging the normalized and unnormalized distribution of line widths in this section, i.e., $G^*(\Gamma;\mathbf{a})$ and $G(\Gamma;\mathbf{a})$.

From Figure 3 we note that the no. 1 datum is negative. Though this is nonphysical, it should be included in our composite $G(\Gamma;\mathbf{a})$ since the no. 4 and no. 7 data resulted from the same fit which produced this negative a_j^*. One other caution about Figure 3 is the apparent resolution obtained by a composite curve overestimates the true resolution of our distribution which is determined when we set $W = 7/2$. For example, the spacing between datum no. 1 and no. 2 represents $W = 5/4$, a resolution much finer than $W = 7/2$. Another caution about this composite distribution is that the number of independent parameters represented in Figure 3 is three, not nine. This means that the nine samplings of $G(\Gamma)$ in Figure 3 are not independent samplings. We emphasize that the reason to form this composite distribution is to achieve an unbiased estimate for $G(\Gamma)$, not a more detailed estimate.

We recall that a plot of $\langle\Gamma\rangle$ vs. concentration should extrapolate to $\langle\Gamma\rangle$ at $c = 0$, a value related to $\langle D_0\rangle_z$ if $P(X) = 1$. Figure 4 displays this zero-concentration extrapolation based on the cumulants method and the multiexponential method. If we take $\langle D_0\rangle_z = 2 \times 10^{-7}$ [cm^2 s^{-1}] we arrive at a 27-nm hydrodynamic radius and a 0.54 value for the ratio of hydrodynamic radius to radius of gyration. These values are of interest when estimating the statistical nature of polymer coils.

4.3. Molecular Weight Distribution. From the $G(\Gamma;\mathbf{a})$ in Figure 3 it is now very simple to calculate the molecular weight distribution, $F_n(M)$, in eq 2-12. The additional information necessary to perform this transform is as follows: (1) the K value, (2) the concentration-dependent term $(1 + k_d c)$, (3) the static light scattering properties $\langle R_g\rangle_z$ and $\langle M\rangle_w$, and (4) the range of intrinsic viscosity scaling exponent α_η from eq 2-22 to be tested. The program utilizes as iterative procedure described in section 2.3 and continues to vary k_D and k_R until the computed $\langle M\rangle_w$ agrees with the measured $\langle M\rangle_w$. In the computations, we have also varied the magnitude of α_η which effects the calculated $\langle M\rangle_n$:$\langle M\rangle_w$:$\langle M\rangle_z$ ratios. This was done to allow an estimate of the sensitivity of our $F_n(M)$ upon the assumption that $\alpha_\eta = 0.72$ (ref 27) for this sample. Our resulting $F_z(M)$, Figure 5, agrees well with the GPC cumulative distribution, $\mathbf{F}_w(M)$, shown in Figure 6. This result confirms that the assumed value for α_η is correct, though we wish to add that the MWD using α_η between 0.65 and 0.75, i.e., good solvent range, result in equally acceptable estimates for the calculated MWD.

The resulting MWD for the sample studied in section 4.2 is shown in Figures 5 and 6. Figure 5 plots $F_z(M)$, that is, the second moment of $F_n(M)$ defined by $F_z(M) = M^2 F_n(M)$, vs. log M. This moment of the MWD is plotted since it is most closely related to $G(D)$, having only included the correction for $P(X)$ via eq 2-2. At first inspection, Figure 5 may appear to be identical with Figure 3, which plotted $G(\Gamma;\mathbf{a})$ vs. log Γ; however, the log M axis has a different spacing than the log Γ axis. We also note that the axis is turned around; the numbering has been kept the same as in Figure 3 so we may follow the effects of each individual contribution to $G(\Gamma;\mathbf{a})$ in $F_z(M)$. By even more careful inspection, we note that $P(X)$ has been corrected for in Figure 5 since the amplitudes at the larger M values are emphasized.

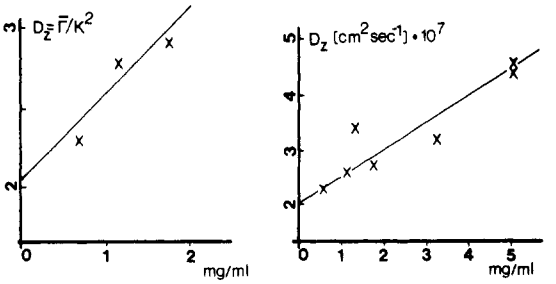

Figure 4. Extrapolation of $\langle\Gamma\rangle$ to zero concentration.

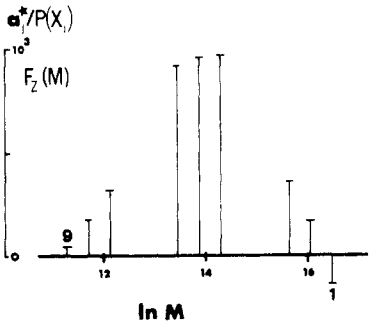

Figure 5. Differential z-average MWD for DSM L-30-4-6 (1.15 mg/mL, 135 °C, TCB solvent, 40° scattering data).

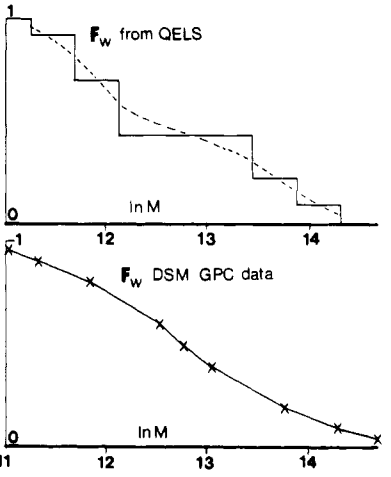

Figure 6. Cumulative w-average MWD for DSM L30-4-6 (from Figure 5) in comparison with the DSM GPC result.

From the dynamic properties of this sample we have, $\langle M\rangle_n = 2.1 \times 10^5$ and $\langle M\rangle_z = 1.40 \times 10^6$. The Dutch State Mines gel permeation chromatography values for these properties are $\langle M\rangle_n = 1.8 \times 10^5$ and $\langle M\rangle_z = 1.50 \times 10^6$. The $\langle M\rangle_w$ value was obtained by static light scattering measurements and was also comparable to a Dutch State Mines value of 5.3×10^5. The moments of our $F_n(M)$ are comparable to those measured by GPC, thus confirming the validity of our method of calculating molecular weight distributions from the combined static and dynamic light scattering data.

We shall go further and inquire how closely does the cumulative weight average MWD, $\mathbf{F}_w(M)$, compare between our method and GPC analysis. Referring back to the definition for a cumulative distribution function, eq

Table II
Parameters Used in Figure 7 for Computing Cumulative Weight-Average MWD of Three Independently Prepared Solutions of DSM L30-4-6

	concn, mg/mL		
	1.75	1.15	0.58
$\langle R_g^2 \rangle$ from Zimm plot (10^{-11} cm^2)	2.5	2.5	2.5
$\langle M \rangle_w$ from Zimm plot	5.7×10^5	5.7×10^5	5.7×10^5
α_D (based on α_η and eq 2-24)	0.57	0.57	0.57
k_D (eq 2-20)	4.35×10^{-4}	4.37×10^{-4}	4.25×10^{-4}
α_R (based on α_η and eq 2-25)	1.15	1.15	1.15
k_R (eq 2-21)	2.34×10^{-18}	2.24×10^{-18}	1.94×10^{-18}
M_z	1.35×10^6	1.40×10^6	1.58×10^6
M_n	2.30×10^5	2.09×10^5	2.87×10^5

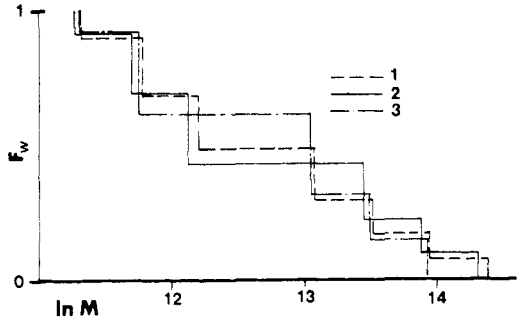

Figure 7. Cumulative w-average MWD for three independent samples (curve 1, 1.75 mg/mL; curve 2, 1.15 mg/mL; curve 3, 0.58 mg/mL). The parameters used are listed in Table II.

2-13, we can calculate $\mathbf{F}_w(M)$ from our discrete distribution since

$$\mathbf{F}_w(M) \equiv \int_M^\infty F_w(M)\, dM \qquad (4\text{-}6)$$

where

$$F_w(M) = MF_n(M) = \sum n_j M_j \delta(M - M_j) \qquad (4\text{-}7)$$

Using our discrete $F_w(M)$ will result in a staircase-shaped $\mathbf{F}_w(M)$ shown in Figure 6. The interpolating line drawn through these steps is then a true estimate of the continuous $\mathbf{F}_w(M)$ measured in GPC experiments. The GPC plot, from DSM data, is shown for comparison in Figure 6. By close inspection we see that our high-M portion of the MWD is less pronounced than the GPC results. This subtle point is probably due to the sample preparation and not to experimental bandwidth problems. The total Γ range being sampled is only 1.3 orders of magnitude wide, whereas our data represent 2 decades of delay time plus a long-time base line point. Dynamic light scattering measures $F_z(M)$ (when $P(X) = 1$), which should, if anything, emphasize the higher M portions of the calculated MWD.

There is one key question for which we can only provide an experimental answer at this point, namely: What are the error bars on our calculated $F_w(M)$? The answer is that the three DSM L30-4-6 samples yield similar $F_w(M)$ plots, with an experimental spread about equal to the step heights as shown in Figure 7. This criterion is not valid if we change the number of datum points in our composite $G(\Gamma;\mathbf{a})$, for increasing beyond nine samplings of $G(\Gamma)$ will result in smaller "step" uncertainties even though the experimental data are no more precise.

Acknowledgment. We gratefully acknowledge support of this work by the U.S. Army Materials and Mechanics Research Center, Watertown, MA, and the U.S. Army Research Office. B.C. thank, R. Koningsveld at DSM, G. Hagnauer at AMMRC, and W. Onclin for their help and useful discussions.

References and Notes

(1) Welzen, Theo "GPC with Online Light Scattering and Online Viscometry for Characterization of Branched Polymers. Application to Low Density Polyethylene Samples". Manuscript of a lecture held on June 10, 1980, at Chalmers University, Goteborg, Sweden.
(2) Chiang, R. *J. Phys. Chem.* **1965**, *69*, 1645.
(3) DiNapoli, A.; Chu, B.; Cha, C. *Macromolecules* **1983**, *15*, 1174.
(4) Chu, B.; Ford, J. R.; Pope, J. "Light Scattering Characterization of Molecular Weight Distributions" In *Conf. Proc. Soc. Plast. Eng., ANTEC 83* **1983**, *26*, 547.
(5) Chandrasekhar, S. *Rev. Mod. Phys.* **1943**, *15*, 1.
(6) Mandel, L. *Proc. Phys. Soc. London* **1959**, *17* 233.
(7) Chu, Ben "Laser Light Scattering"; Academic Press: New York, 1974.
(8) Siegert, A. MIT Radiation Laboratory Report No. 465, 1943.
(9) Glauber, R. J. *Phys. Rev.* **1963**, *132*, 2766.
(10) Oliver, C. J. In "Scattering Techniques Applied to Supramolecular and Nonequilibrium Systems"; Chen, S. H., Chu, B, Nossal, R., Eds.; Plenum Press: New York, 1981; pp 87–160. (All references to E. Jakeman from this source are of interest.)
(11) Huglin, M. B., Ed. "Light Scattering from Polymer Solutions"; Academic Press: New York, 1972).
(12) Kratohvil, P. Chapter 7 in ref 11.
(13) Zimm, B. H. *J. Chem. Phys.* **1948**, *16*, 1093.
(14) Cantow, H. S. *Makromol. Chem.* **1956**, *18/19*, 367.
(15) Coumou, D. J.; Makor, E. L.; Hijmans, J. *Trans. Faraday Soc.* **1964**, *60*, 1539.
(16) Coumou, D. J. *J. Colloid Sci.* **1960**, *15*, 408.
(17) Tomimatsu, Y.; Palmer, K. J. *J. Polym. Sci.* **1964**, *35* (129), 549.
(18) Ehl, J.; Loucheux, C.; Reiss, C.; Benoit, H. *Makromol. Chem.* **1964**, *75*, 35.
(19) Carr, C. I. Ph.D. Dissertation, University of California, 1949.
(20) Chu, B.; Onclin, W.; Pope, J. "Report on Polyethylene 1981", unpublished results.
(21) Ultimaya, H. In Chapter 4 of ref 11.
(22) Berne, B. J.; Pecora, R. "Dynamic Light Scattering"; Wiley: New York, 1976; Chapter 8.
(23) Reference 22, section 5.9.
(24) Jakeman, E.; Pike, E. R.; Swain, S. *J. Phys. A: Gen. Phys.* **1971**, *4*, 517.
(25) Lawson, C. L.; Hanson, R. J. "Solving Least Squares Problems"; Prentice-Hall: Englewood Cliffs, NJ, 1974. We have utilized the LSVDF singular-valued decomposition routine from this text as implemented by the International Math and Statistics Library, Houston, TX.
(26) "Proceedings of the 5th International Conference on Photon Correlation Techniques in Fluid Mechanics"; Schulz-DuBois, E. O., Ed.; Springer-Verlag: New York, 1983.
(27) Cervenka, A. *Makromol. Chem.* **1973**, *170* 239.
(28) Flory, P. J. "Principles of Polymer Chemistry", Cornell University Press: Ithaca, NY, 1971. See also: de Gennes, P.-G. "Scaling Concepts in Polymer Physics"; Cornell University Press: Ithaca, NY, 1979.
(29) Beilstein, "Handbook of Organic Compounds", B 5/2 664, 1,2,4-Trichlor-benzol, $C_6H_3Cl_3$.
(30) Griffing, V.; Cargyle, M.; Corvese, L.; Eby, D. *J. Phys. Chem.* **1954**, *58*, 1054.
(31) McWhirter, J. G.; Pike, E. R. *J. Phys. A* **1978**, *11*, 1729.
(32) Provencher, S. W. *Biophys. J.* **1976**, *16*, 27; *J. Chem. Phys.* **1976**, *64*, 2772; *Makromol. Chem.* **1979**, *180*, 201.
(33) Miller, G. F., "Numerical Solution of Integral Equations"; Delves, L. M., Walsh, J., Eds.; Oxford University Press: London, 1974.
(34) Bertero, M.; Boccaci, P.; Pike, E. R. *Proc. R. Soc. London, Ser. A* **1982**, *383*, 15.
(35) Ostrowski, N.; Sornette, D.; Parker, P.; Pike, E. R. *Opt. Acta* **1981**, *28*, 1059.
(36) Koppel, D. E. *J. Chem. Phys.* **1972**, *57*, 4814.